HHS Public Access

Author manuscript

J Biomed Mater Res A. Author manuscript; available in PMC 2017 February 01.

Published in final edited form as:

J Biomed Mater Res A. 2016 February ; 104(2): 347–356. doi:10.1002/jbm.a.35570.

Biphasic responses of human vascular smooth muscle cells to magnesium ion

Jun Ma[1,2], **Nan Zhao**[1,2], and **Donghui Zhu**[1,2]

[1]Department of Chemical, Biological and Bio-Engineering, North Carolina Agricultural and Technical State University, Greensboro, North Carolina 27411

[2]NSF-ERC For Revolutionizing Metallic Biomaterial, North Carolina Agricultural and Technical State University, Greensboro, North Carolina 27411

Abstract

Magnesium-based alloys are promising in biodegradable cardiovascular stent applications. The degradation products of magnesium stents may have significant impacts on the surrounding vascular cells. However, knowledge on the interactions between magnesium ion and vascular cells at the molecular and cellular levels is still largely missing. Vascular smooth muscle cell (SMC) plays an important role in the pathogenesis of restenosis and wound healing after stent implantation. This study evaluated the short-term effects of extracellular magnesium ion (Mg^{2+}) on the cellular behaviors of SMCs. Cellular responses to Mg^{2+} were biphasic and in a concentration-dependent manner. Low concentrations (10 m*M*) of Mg^{2+} increased cell viability, cell proliferation rate, cell adhesion, cell spreading, cell migration rate, and actin expression. In contrast, higher concentrations (40–60 m*M*) of Mg^{2+} had deleterious effects on cells. Gene expression analysis revealed that Mg^{2+} altered the expressions of genes mostly related to cell adhesion, cell injury, angiogenesis, inflammation, coagulation, and cell growth. Finding from this study provides some valuable information on SMC responses toward magnesium ions at the cellular and molecular levels, and guidance for future controlled release of magnesium from the stent material.

Keywords

magnesium ion; cardiovascular stent; smooth muscle cell; cell morphology; cell migration

INTRODUCTION

Magnesium-based alloys have been demonstrated promising in cardiovascular stent applications because of their biodegradability and bioabsorbtion.[1–6] *In vivo* studies have also shown the advantages of magnesium-based stents, such as complete and rapid endothelialization, low neointima proliferation and minimum inflammatory changes.[1,5,6] The fact that magnesium is the second most abundant intracellular divalent cation makes it

Correspondence to: D. Zhu; ; Email: dzhu@ncat.edu.

an appealing candidate as degradable biomaterial. Moreover, it is the cofactor for many enzymes and plays structural roles in the cell membrane and chromosomes.[7] However, low corrosion resistance is one of main concerns in magnesium-based stent application. Rapid corrosion makes magnesium alloys fail to fulfill their remedying functions, that is, supporting the remodeling process and the healing process of the damaged tissues.[8] In fact, fast degradation of magnesium-based implants may lead to a relatively high local extracellular magnesium concentration around the implant.[7] Thus, the cellular responses to high extracellular Mg^{2+} are essential to evaluate the biocompatibility of magnesium alloys and the healing process. Unfortunately, little is known about the interactions between vascular cells and Mg^{2+} at the cellular and molecular levels to date.

Normal ionized magnesium concentration in serum is 0.54–0.67 m*M*.[9] However, when magnesium-based stent is implanted, the shear stress induced by restored blood flow will increase the degradation rate of magnesium stent.[10,11] The continuous blood flow might dilute the accumulated Mg^{2+} concentration, but increased corrosion rate by shear stress may also promote the accumulation of Mg^{2+}. High extracellular Mg^{2+} could still be accumulated in the local microenvironment around the stent in a short period of time.

We have studied the effects of Mg, Ca, Zn, Al and rare earth elements including yttrium (Y), dysprosium (Gy), neodymium (Nd), and gadolinium (Gd) on cellular responses of endothelial cells previously.[12] To have a better understanding of how Mg ion affects the local tissues for stent application, we further investigated the effects of Mg^{2+} on human primary SMCs in this study. Vascular smooth muscle cell (SMC) plays important roles in the pathogenesis of restenosis after stent application and wound healing.[13,14] As part of responses to stent implantation-induced vascular injury, SMCs migrate from media to the intima and proliferate, leading to neointimal thickening and restenosis.[15] Vascular SMCs can retain remarkable plasticity and undergo dedifferentiation, responding to stimuli. SMCs can enable the efficient repair of the vasculature after injury.[14] Under normal conditions, vascular SMCs exhibit a contractile phenotype, characterized by low levels of proliferative activities.[15] During migration and proliferation processes, SMCs can switch from a contractile to a synthetic phenotype,[13] and the phenotype switch is associated with morphology change.[16,17]

Here, we comprehensively studied the short-term cellular responses of SMCs under the influence of Mg ion for up to 24 h. Cell adhesion, cell viability, cell proliferation, lactate dehydrogenase (LDH) cytotoxicity, cell spreading, cytoskeleton reorganization, and gene expression profiles were explored.

EXPERIMENTAL

Ion solution preparation

Stock solutions of 1 *M* magnesium chloride ($MgCl_2$) and 1 *M* sodium chloride (NaCl) were prepared by dissolving $MgCl_2$ and NaCl into deionized water. Then the solutions were centrifuged (Biofuge Stratos, Thermo Electron Corporation) and filtered by 0.22 μm filter (BD Biosciences). The stock solution was sterilized by autoclave (Harvey Sterile-Max, Thermo Scientific). After that, the solutions were stored in 4°C refrigerator until use. Before

using, the stock solutions were diluted into different concentrations with smooth muscle culture medium (SMCM, ScienCell). The pH of diluted solutions was measured by Fisher Science Education pH Meter (Fisher Scientific).

Cell culture

Primary human aortic smooth muscle cells (HASMCs, Scien-Cell) were expended in 75 cm^2 flask (BD Bioscience) with SMC medium containing 2% fetal bovine serum (FBS, Scien-Cell), 1% smooth muscle cell growth supplement (SMCGS, ScienCell) and 1% penicillin/streptomycin solution (P/S, ScienCell). Cells were incubated at 37ºC, 5% CO_2 and 95% relative humidity. After cells reached 90% confluence, they were washed by 1× DPBS (MP Biomedicals), detached by Trypsin/EDTA solution (Life Technologies), and counted with 0.4% trypan blue stain (Gibco, Life Technologies) by a hemocytometer (Bright-Line, Hausser Scientific). Cells at passages of 4–6 were used in this study.

Cell viability test

The cell viability was assessed by 3-(4,5-dimethylthiazol-2-yl)–2,5-diphenyltetrazolium bromide test (MTT test). SMCs were seeded into a 96-well plate at density of 5000 cells/well and allowed to attach for 24 h. Then the medium was replaced by fresh culture medium supplemented with different ion solutions (0–60 m*M*). After 24 h, the ion solutions were replaced by fresh medium. Then 10 μL of the 12 m*M* MTT solution was added to each well and incubated at 37ºC for 4 h. After the incubation, 100 μL SDS-HCl solution was added to each well and incubated for another 4 h. Then the absorbance was measured at 570 nm by a microplate reader (Molecular Devices). Culture medium with and without cells were used as positive and negative control, respectively. The cell viability was determined by the following formula:

$$\text{Cell viability} = (\text{ABS}_{\text{sample}} - \text{ABS}_{\text{negative}}) / (\text{ABS}_{\text{positive}} - \text{ABS}_{\text{negative}})$$

Cell proliferation test

The cell proliferation was evaluated by BrdU cell proliferation kit (Cell Signaling). SMCs were seeded into a 96-well plate at density of 5000 cells/well and incubated for 24 h to allow attachment. Then medium was replaced by fresh culture medium supplemented with different ion solutions (0–60 m*M*) and incubated for another 24 h. After that, 10 μL 10× BrdU solution was added to each well and incubated for 3 h. After the incubation, the solutions were removed. 100 μL fixing/denaturing solution was added to each well and the plate was kept at room temperature for 30 min. Then the solution was removed and 100 μL 1×detection antibody solution was added to each well. The plate was kept at room temperature for 1 h. After that, the solution was removed and the plate was washed by 1× wash buffer for three times. Then 100 μL 1× HRPconjugated antibody solution was added to each well and the plate was kept at room temperature for 30 min. Then the plate was washed three times by 1× wash buffer. After washing, 100 μL TMB substrate was added to each well and incubated at room temperature for 30 min. Finally, 100 μL stop solution was added to each well and the absorbance was read at 450 nm by a microplate reader (Molecular

Devices). The culture medium with and without cells were used as positive and negative control, respectively. The cell proliferation was calculated by the following formula:

$$\text{Cell proliferation} = (\text{ABS}_{\text{sample}} - \text{ABS}_{\text{negative}}) / (\text{ABS}_{\text{positive}} - \text{ABS}_{\text{negative}})$$

LDH cytotoxicity test

SMCs were seeded into a 96-well plate at 5000 cells/well and incubated for 24 h. After the incubation, culture medium was replaced by 200 μL fresh culture medium supplemented with different ion solutions (0–60 m*M*) and incubated for another 24 h. Then 100 μL solution supernatant was removed and transferred to a corresponding 96-well plate. To determine the LDH activity in the supernatant, 100μL reaction mixture was added to each well and mixed thoroughly. Then the plate was kept at room temperature for 30 min. After the incubation, absorbance was measured at 490 nm (Molecular Devices). The high control and low control were SMCs incubated with 1% Triton X-100 medium solution and SMCs without any treatment. The LDH cytotoxicity was determined by the following formula:

$$\text{LDH cytotoxicity} = (\text{ABS}_{\text{sample}} - \text{ABS}_{\text{low}}) / (\text{ABS}_{\text{high}} - \text{ABS}_{\text{low}})$$

Cell adhesion test

SMCs were mixed with fresh culture medium supplemented with different ion solutions (0–60 m*M*) and seeded into a 24-well plate. The final cell density was 50,000 cell/well. The cells were allowed to attach for 2 and 6 h. After 2 and 6 h, the medium was removed and the plate was washed three times by 1× DPBS (MP Biomedicals). Cells were fixed by 4% paraformaldehyde (Boston BioProducts). The images of adhesive cells were taken by a microscope (EVOS, AMG) and the pictures were analyzed by Image J (NIH). At least 10 different images were used in adhesive cell density calculation for each concentration group.

Cell spreading

SMCs were seeded into 24-well plates at density of 50,000 cells/well. The cells were incubated with fresh culture medium supplemented with different ion solutions (0, 20, and 60 m*M*). At 0, 2, 4, 6, 8, and 10 h, cells were stained by calcein AM (Life Technologies) and imaged by phase contrast microscope (EVOS, AMG). Cell area and perimeter were measured by Image J (NIH). At least 50 cells were measured for each magnesium ion concentration.

Cell migration

SMCs were seeded into a 24-well plate and after the cells formed a monolayer, the medium was removed. A p200 pipette tip was used to create a scratch. The debris were washed by DPBS and removed. Then fresh culture medium supplemented with different ion solutions (0–60 m*M*) were added to each well and incubated at 37ºC, 5% CO_2 and 95% relative humidity. Images were taken at 0 h and 6 h by EVOS microscopy (AMG) and the pictures were analyzed by Image J (NIH). At least 10 different fields were chosen for each concentration group. The migration rate (MR) was calculated by the following formula:

$$\mathrm{MR} = (\text{Initial width} - \text{current width}) / \text{Recovery time}$$

Cytoskeleton staining and cell morphology

SMCs were seeded onto cover glasses in a 24-well plate at cell density of 25,000 cells/well and incubated with fresh culture medium supplemented with different ion solutions (0, 20, and 60 m*M*) for 24 h. Then culture medium was removed and cells were fixed and permeabilized by ImageiT Fixation Permeabilization Kit (Life Technologies). Then one drop of Actin Green 488 ReadyProbes Reagent was added to each cover class and incubated at room temperature for 30 min. The cells were washed three times by DPBS and one drop of SlowFade® Gold antifade reagent with DAPI (Molecular probes, Life Technologies) was added to the glass slide and the cover glass was inversely placed on the reagent. Then the glass slides were sealed by Cover-Grip Coverslip Sealant (Biotuim) and were incubated at room temperature overnight in dark. Images were taken by a phase contrast microscope (EVOS, AMG) and analyzed by Image J (NIH). For cell morphology characterization, at least 30 different cells were analyzed for each concentration group.

GENE EXPRESSION PROFILE

Total RNA isolation

SMCs were seeded into 60 mm petri dishes and when a monolayer was formed, culture medium was replaced with SMCM, supplemented with 20 m*M* or 60 m*M* $MgCl_2$ solutions. After 24 h, the medium was removed and cells were washed by DPBS for three times. Then total RNA was isolated by RNeasy Mini Kit (Qiagen) following the manufacturer's protocol. The quality and concentration of total RNA were determined by a spectrophotometer (Nanodrop 2000). A_{260}/A_{280} ratio was between 2.02 and 2.06 and the A_{260}/A_{230} ratio was between 2.0 and 2.29.

RT-PCR

500 ng total RNA were reversely transcripted into cDNA by RT^2 First Strand Kit (Qiagen), according to the manufacturer's protocol. RT-PCR was performed in a CFX96 Touch RT-PCR Detection System (Bio-Rad) using microarray (Qiagen). The vascular gene array plate includes 84 functional genes, 5 housekeeping genes, 1 genomic DNA control, 3 reverse transcription controls, and 3 positive PCR controls. Then cDNA was mixed with RT^2 SYBR Green Master Mix (Qiagen) and RNase-free water. Then 25 μL of the mixture was added to 96-well PCR array plate. After 10 min incubation at 95ºC, cDNA was amplified according to the following parameters: denaturing for 15 s at 95ºC, then annealing for 1 min at 60ºC. The cDNA amplification was performed for 40 cycles. After the amplification, Ct values were collected and analyzed by Bio-Rad CFX Manager 3.1 (Bio-Rad). The threshold cycle was 35. ΔΔCt method was used to calculate gene expression fold change.

Statistical analyses

All data were presented as mean±standard deviation (SD). The statistical studies were performed by analysis of variance or one-tailed Student's *t test* (Prism 5, Graph Pad Software). $p<0.05$ was considered statistically significant.

RESULTS

Cell viability

Cell viability was examined with a serial of Mg ion concentrations. For all the diluted solutions, no significant pH changes were observed after incubation. The NaCl solution, with the same chloride ion concentration as $MgCl_2$ solutions, was used to exclude the effects of chloride ions. As shown in Figure 1(a), the viability of SMCs increased when cultured in lower concentrations of $MgCl_2$ solution (10–40 m*M*). At higher Mg^{2+} concentrations (50–60 m*M*), cell viability was inhibited. In contrast, the control NaCl solution had no effect on cell viability up to 140 m*M* [Fig. 1(b)].

Cell proliferation

A concentration gradient of Mg ion was also used to check on cell proliferation. As shown in Figure 2, cell proliferation rate of SMCs increased at lower Mg^{2+} concentrations and then decreased at higher concentrations. Within 10–20 m*M* concentration range, cell proliferation rate was enhanced with increasing Mg^{2+} concentration whereas within 40–60 m*M* concentration range, cell proliferation rate was decreased with increasing Mg^{2+} concentration, and was significantly inhibited at 60 m*M* Mg^{2+}.

LDH cytotoxicity

LDH assay checks on the cell plasma membrane integrity. LDH release was enhanced at first for low Mg^{2+} concentrations (10–20 m*M*) and then decreased with increasing Mg^{2+} concentrations (30–50 m*M*). Surprisingly, at 60 m*M*, the LDH release was again increased to 14±5%, comparable to the value of 15±3% at 20 m*M*. For all Mg^{2+} concentrations, LDH release was significantly higher than the control group (Fig. 3).

Cell adhesion

Next we explored the cell adhesion at different time points with an Mg ion concentration gradient. At 2 h, 10 m*M* Mg^{2+} enhanced the adhesion of SMCs significantly while cell adhesion was significantly inhibited within 30–60 m*M* concentration range. At 6 h, 10 and 20 m*M* Mg^{2+} increased adherent density of SMCs, and in the contrast, cell adhesion was significantly inhibited within 40–60 m*M* concentration range. In addition, more SMCs were attached to the plate at 6 h compared to that of 2 h (Fig. 4).

Cell spreading

Mg ion also influenced cell spreading. Around 8 h, cell spreading reached a steady state. In the cell spreading process, 20 m*M* Mg^{2+} increased cell area [Fig. 5(a)] and cell perimeter [Fig. 5(b)], compared to that of the control group. Interestingly, for 60 m*M* Mg^{2+}, cell area [Fig. 5(a)] and cell perimeter [Fig. 5(b)] were increased at first, and then decreased slightly.

Cell migration

The relationship between cell migration rate and Mg^{2+} concentrations was in a bell-shape distribution. At 6 h, cell migration rate of SMCs was significantly enhanced by lower Mg^{2+} concentrations up to 30 m*M* and then inhibited with further increased concentration (40–60 m*M*; Fig. 6).

Cell morphology and cytoskeleton staining

The representative images of SMCs treated with different Mg^{2+} concentrations were shown in Figure 7(a). After 24 h treatment, cell spreading was enhanced by Mg^{2+}. At 20 m*M* Mg^{2+}, cell area was increased significantly compared to untreated control [Fig. 7(b)]. Cell perimeter was increased at 20 m*M* Mg^{2+} whereas decreased at 60 m*M* Mg^{2+} significantly [Fig. 7(c)]. The aspect ratio was enhanced at 20 m*M* Mg^{2+} [Fig. 7(d)]. Compared to the untreated control group, cells had a smaller circularity for 20 m*M* Mg^{2+} but a much larger circularity for 60 m*M* Mg^{2+} [Fig. 7(e)]. The actin fluorescence intensity was enhanced significantly at 20 m*M* Mg^{2+} while a significant decrease was observed at 60 m*M* Mg^{2+} [Fig. 7(f)].

Gene expression profiles

To evaluate how Mg^{2+} alters gene expression profile, here we used a microarray with 84 functional genes. As shown in Figure 8(a,b), the gene expression regulations seemed more considerable at 60 m*M* Mg^{2+}, compared to 20 m*M* Mg^{2+}. The most affected functions were cell adhesion, cell injury, cell growth, angiogenesis, inflammation, vessel tone, and coagulation [Fig. 8(c,d)]. 24 genes were altered around or more than twofold. Among all the significantly regulated genes, SERPINE1, PTGS2, IL1B, and HMOX1 were altered more than three times. AGT, PDGFRA, PTGS2, and THDB were upregulated at least twofold, while ICAM1, PLG, SELPLG, and SERPINE1 were downregulated at least twofold at 20 m*M* Mg^{2+}. For 60 m*M* Mg^{2+}, ADAM17, AGTP1, F3, FAS, FGF2, HMOX1, IL11, IL1B, MMP1, PF4, PTGS2, SELPLG, SERPINE1, SPHK1, and TGFB1 were upregulated at least twofold. In contrast, BCL2, CCL2, ICAM1, PLG, and VCAM1 were downregulated at least twofold at 60 m*M* Mg^{2+} [Fig. 8(e)].

DISCUSSION

Stent implantation has been one of the most effective means for cardiovascular diseases treatment.[18] Magnesium-based alloys have been frequently explored for stent application because of biodegradation. Some animal experiments[1,5,6] and clinical results[19–22] suggested the feasibility and potential of magnesium-based alloys. In this study, we evaluated the acute effects of extracellular Mg^{2+} on the cellular responses of SMCs. We found after 24 h incubation, up to 50 m*M* of Mg^{2+} had no significant adverse effects on SMC viability and proliferation rate. These results were consistent with the study conducted by Drynda et al.,[23] which found that up to ~41.6 m*M*, Mg^{2+} showed no significant effects on the metabolic activity of SMCs. Another study showed that up to 50 m*M*, Mg^{2+} had no significant effects on SMCs viability, but SMCs proliferation rate was only ~50% of control at 50 m*M*.[24] The discrepancy in proliferation rate between these studies is probably due to other factors, such as cell passage and cell type variations.

The movement of SMCs inwardly from the media to intima depends on the ability of the cells to adhere, migrate, and proliferate.[25] Integrins play important roles in the adhesion of a cell to its environment, mediating the assembly of multimolecular complexes that bridge between the extracellular matrix (ECM) and cytoskeleton and focal adhesion sites.[26,27] By influencing the cytoskeleton, integrins can stabilize cell adhesion and regulate the shape, morphology, and movement of cells.[27] ITGA5, ITGAV, and ITGB3 are some genes involved in integrin synthesis. In this study, at 20 m*M* Mg^{2+}, ITGA5 was downregulated and ITGAV and ITGB3 were upregulated. In contrast, at 60 m*M* Mg^{2+}, only ITGAV was upregulated. The expression profiles of more than 40 genes related to cell adhesion were altered when SMCs were treated with Mg^{2+}. Taken together, the overall cell adhesion behavior was promoted at lower Mg^{2+} concentrations (10–20 m*M*) and inhibited at higher Mg^{2+} concentrations.

Cell spreading is closely related to cellular biomechanics and cell growth.[28] Cell spreading on adhesive proteins is accompanied by changes in structure and composition of the cytoskeleton.[29] In addition, cell spreading is also associated with stress fiber formation[30] and cytoskeleton tension. [30,31] Previous studies showed that increasing spreading without changing ECM contact area and growth factor signaling constant was sufficient to promote endothelial cell proliferation, while preventing cells from spreading had the opposite effect,[28] which indicated that biophysical signals associated with cell spreading were required for cell growth.[28,31] In another study, human bone-derived cells were believed to have a more pronounced spreading grown on Mg^{2+}-modified alumina.[32] In our study, cell spreading was promoted at 20 m*M* Mg^{2+} and inhibited at 60 m*M* Mg^{2+}. The result was consistent with cell proliferation rate and actin expression level at these two concentrations.

SMC proliferation and migration from media to intima contribute to restenosis.[14,33] The matrix metalloproteinases (MMPs) are proteases with different specificities for cleaving ECM components. The proliferation and migration of SMCs are closely associated with the simulation of MMP-2 production and increased MMP-2 expression has been reported in atherosclerotic plaques.[34] In this study, MMP-2 was significantly upregulated at 20 m*M* Mg^{2+}, which was consistent with the enhanced cell migration rate.

LDH is a cytosolic enzyme that can leak into the culture medium when cell membrane is damaged.[8] Therefore, the activity of LDH in the culture medium could reflect the cytotoxicity of materials[35] and LDH test has been widely used in biocompatibility evaluation for magnesium-based biomaterials.[36–40] In this study, at low Mg^{2+} concentrations, significantly higher LDH cytotoxicity than that of control was also observed. It was probably because at low Mg^{2+} concentrations, SMC proliferation rate was enhanced and there were more cells in the low Mg^{2+} concentration-treated group, leading to an increase in spontaneous LDH release. Possible explanation for decrease in LDH cytotoxicity for treatment with 20–50 m*M* Mg^{2+} was that high concentration of extracellular Mg^{2+} may inactivate the LDH released in the medium.[9] At 60 m*M* Mg^{2+}, the cell membrane was damaged and LDH was released into the culture medium completely. Results showed the LDH cytotoxicity test might not be suitable for evaluating the biocompatibility of magnesium-based alloys.

We also investigated the cytoskeleton reorganization and cell morphology at 20 m*M* and 60 m*M* Mg^{2+}. Cytoskeleton carries out three main functions: organizing the contents of cell spatially; connecting the cell to external environment physically and biochemically; generating forces to enable cell to move and change shape.[41] Cell shape changes rely on dynamic reorganization of the actin cytoskeleton.[42] The reorganization of actin fiber changed the morphology of SMCs in this study. When treated with 20 m*M* Mg^{2+}, cells were in elongated shape, while cells treated with 60 m*M* Mg^{2+} tended to be in round shape, compared to the control group. The elongated cell morphology resembles the natural state of SMCs *in vivo*, which might suggest the beneficence of low concentrations of Mg^{2+}. The morphology changes might also indicate that low concentrations of Mg^{2+} could promote SMC differentiation while high concentrations of Mg^{2+} inhibit the differentiation process. Since actin is required for SMC contraction,[43] the enhanced expression level of actin at low Mg^{2+} concentrations might also suggest the phenotype switch from synthetic to contractile phenotype. However, the expression of some contractile phenotype markers, such as smooth muscle α-actin (SM α-actin), SM22 α, and calponin 1, should be identified in the future study to further confirm this phenotype switch.

Mg^{2+} mainly influenced cell adhesion, cell injury, cell growth, angiogenesis, and inflammation functions of SMCs. The expressions of about 24 genes were altered at least twofold. The fold changes of F3, HMOX1, IL1B, PTGS2, and SERPINE1 were more than 3 times. F3 gene encodes for tissue factor, which is a transmembrane protein that mediates coagulation, hemostasis, and arterial thrombosis.[44] 60 m*M* Mg^{2+} upregulated F3 gene significantly, while 20 m*M* Mg^{2+} had no significant effects on F3 gene expression. SERPINE 1 gene was significantly downregulated at 20 m*M* Mg^{2+} and upregulated at 60 m*M* Mg^{2+}. The plasminogen activator inhibitor-1 (PAI-1), encoded by SERPINE 1, is the principal inhibitor of tissue plasminogen activator (tPA) and urokinase (uPA), hence inhibiting blood clots degradation.[45] The downregulation of SERPINE 1 at low Mg^{2+} concentrations and upregulation at high Mg^{2+} concentrations might be the indicative of the beneficent effects of low concentrations of Mg^{2+} on coagulation. Studies[46,47] also showed the anticoagulation properties at various low Mg^{2+} concentrations. These results indicated that the low concentrations of Mg^{2+} had better hemocompatibility. However, platelet adhesion test on Mg-based alloys had found that both alloys with high and low corrosion rate had anticoagulation properties.[3,48,49] Slowly corroded magnesium alloys had low levels of platelet aggregation, which was consistent with our observation.

Heme oxygenase-1(HO-1), encoded by HMOX1 gene, is a stress-responsive enzyme and can degrade free heme, yielding carbon monoxide (CO), iron, and biliverdin. HMOX1 serves as a protective gene by virtue of its anti-inflammatory, antiapoptotic, and antiproliferation actions.[50] The antiproliferation effects of HO-1 on SMC is exerted by catalyzing release of CO, which inhibits the mitogenic activity of SMCs.[51] High concentrations of Mg^{2+} upregulated HMOX1 gene, which might explain the decreased SMC proliferation rate at 60 m*M* Mg^{2+}.

IL1B gene encodes for interleukin-1β (IL-1β), a major mediators of inflammatory responses in atherosclerotic lesions.[52] Monocytes, macrophages, T cells and mast cells synthesize a variety of proinflammatory cytokines, including IL1β, IL6, and tumor necrosis factor α,

contributing to the initiation, development and rupture of atherosclerotic plaques. [53] Besides its important role in inflammation responses, IL 1β can also enhance the expression of vascular endothelial growth factor (VEGF) in smooth muscle cell,[54] indicating the angiogenesis potential of IL-1B. PTGS2 gene expression simulated by 60 m*M* Mg^{2+} was more than 6 fold. It is also believed to play an important role in inflammation.[55] The significant changes of these two inflammation-related genes might indicate that Mg^{2+} is essential in inflammation responses.

CONCLUSION

The cellular responses of SMCs to extracellular Mg^{2+} were in a dose-dependent manner. Lower concentrations (10 m*M*) of Mg^{2+} had beneficial effects on cellular behaviors, while high concentrations (40–60 m*M*) of Mg^{2+} had adverse effects. The gene expression profiles showed that Mg^{2+} pronouncedly altered the expression of genes related to coagulation, inflammation and cell proliferation. In addition, high concentrations of Mg^{2+} were likely to induce coagulation and inflammation, and inhibit SMC proliferation. At low concentration, Mg^{2+} seemed to increase cell proliferation and cell migration rate. This study provides some valuable information on how Mg ion released from Mg-based stents degradation may affect SMC-associated restenosis and thrombosis.

Acknowledgments

Contract grant sponsor: National Institute of General Medical Sciences of the National Institutes of Health; contract grant number: SC3GM113762

Contract grant sponsor: National Science Foundation Engineering Research Center-Revolutionizing Metallic Biomaterials (ERC-RMB) at North Carolina A&T State University

References

1. Di Mario C, Griffiths H, Goktekin O, Peeters N, Verbist J, Bosiers M, Deloose K, Heublein B, Rohde R, Kasese V. Drug-eluting bioabsorbable magnesium stent. J Interventional Cardiol. 2004; 17:391–395.
2. Erbel R, Di Mario C, Bartunek J, Bonnier J, de Bruyne B, Eberli FR, Erne P, Haude M, Heublein B, Horrigan M. Temporary scaffolding of coronary arteries with bioabsorbable magnesium stents: A prospective, non-randomised multicentre trial. Lancet. 2007; 369:1869–1875. [PubMed: 17544767]
3. Gu X, Zheng Y, Cheng Y, Zhong S, Xi T. In vitro corrosion and biocompatibility of binary magnesium alloys. Biomaterials. 2009; 30:484–498. [PubMed: 19000636]
4. Hänzi AC, Gerber I, Schinhammer M, Löffler JF, Uggowitzer PJ. On the in vitro and in vivo degradation performance and biological response of new biodegradable Mg–Y–Zn alloys. Acta Biomater. 2010; 6:1824–1833. [PubMed: 19815099]
5. Heublein B, Rohde R, Kaese V, Niemeyer M, Hartung W, Haverich A. Biocorrosion of magnesium alloys: A new principle in cardiovascular implant technology? Heart. 2003; 89:651–656. [PubMed: 12748224]
6. Waksman R, Pakala R, Kuchulakanti PK, Baffour R, Hellinga D, Seabron R, Tio FO, Wittchow E, Hartwig S, Harder C. Safety and efficacy of bioabsorbable magnesium alloy stents in porcine coronary arteries. Catheter Cardiovasc Interv. 2006; 68:607–617. [PubMed: 16969879]
7. Wu L, Luthringer BJ, Feyerabend F, Schilling AF, Willumeit R. Effects of extracellular magnesium on the differentiation and function of human osteoclasts. Acta Biomater. 2014; 10:2843–2854. [PubMed: 24531013]

8. Purnama A, Hermawan H, Couet J, Mantovani D. Assessing the biocompatibility of degradable metallic materials: State-of-the-art and focus on the potential of genetic regulation. Acta Biomater. 2010; 6:1800–1807. [PubMed: 20176149]
9. Swaminathan R. Magnesium metabolism and its disorders. Clin Biochem Rev. 2003; 24:47. [PubMed: 18568054]
10. Hermawan H, Purnama A, Dube D, Couet J, Mantovani D. Fe–Mn alloys for metallic biodegradable stents: Degradation and cell viability studies. Acta Biomater. 2010; 6:1852–1860. [PubMed: 19941977]
11. Wang J, Giridharan V, Shanov V, Xu Z, Collins B, White L, Jang Y, Sankar J, Huang N, Yun Y. Flow-induced corrosion behavior of absorbable magnesium-based stents. Acta Biomater. 2014; 10:5213–5223. [PubMed: 25200844]
12. Zhao N, Zhu D. Endothelial responses of magnesium and other alloying elements in magnesium-based stent materials. Metallomics. 2015; 7:113–123.
13. Hao H, Gabbiani G, Bochaton-Piallat M-L. Arterial smooth muscle cell heterogeneity implications for atherosclerosis and restenosis development. Arterioscler Thromb Vasc Biol. 2003; 23:1510–1520. [PubMed: 12907463]
14. Marx SO, Totary-Jain H, Marks AR. Vascular smooth muscle cell proliferation in restenosis. Cir Cardiovasc Interv. 2011; 4:104–111.
15. Inoue T, Node K. Molecular basis of restenosis and novel issues of drug-eluting stents. Cir J. 2009; 73:615–621.
16. Hao H, Ropraz P, Verin V, Camenzind E, Geinoz A, Pepper MS, Gabbiani G, Bochaton-Piallat M-L. Heterogeneity of smooth muscle cell populations cultured from pig coronary artery. Arterioscler Thromb Vasc Biol. 2002; 22:1093–1099. [PubMed: 12117722]
17. Rensen S, Doevendans P, Van Eys G. Regulation and characteristics of vascular smooth muscle cell phenotypic diversity. Neth Heart J. 2007; 15:100–108. [PubMed: 17612668]
18. Fattori R, Piva T. Drug-eluting stents in vascular intervention. Lancet. 2003; 361:247–249. [PubMed: 12547552]
19. Ghimire G, Spiro J, Kharbanda R, Roughton M, Barlis P, Mason M, Ilsley C, Di Mario C, Erbel R, Waksman R. Initial evidence for the return of coronary vasoreactivity following the absorption of bioabsorbable magnesium alloy coronary stents. Eurointervention. 2009; 4:481–484. [PubMed: 19284070]
20. Haude M, Erbel R, Erne P, Verheye S, Degen H, Böse D, Vermeersch P, Wijnbergen I, Weissman N, Prati F. Safety and performance of the drug-eluting absorbable metal scaffold (DREAMS) in patients with de-novo coronary lesions: 12 month results of the prospective, multicentre, first-in-man BIOSOLVE-I trial. Lancet. 2013; 381:836–844. [PubMed: 23332165]
21. Schranz D, Zartner P, Michel-Behnke I, Akintürk H. Bioabsorbable metal stents for percutaneous treatment of critical recoarctation of the aorta in a newborn. Catheter Cardiovasc Interv. 2006; 67:671–673. [PubMed: 16575923]
22. Zartner P, Cesnjevar R, Singer H, Weyand M. First successful implantation of a biodegradable metal stent into the left pulmonary artery of a preterm baby. Catheter Cardiovasc Interv. 2005; 66:590–594. [PubMed: 16206223]
23. Drynda A, Hassel T, Hoehn R, Perz A, Bach FW, Peuster M. Development and biocompatibility of a novel corrodible fluoride-coated magnesium-calcium alloy with improved degradation kinetics and adequate mechanical properties for cardiovascular applications. J Biomed Mater Res Part A. 2010; 93:763–775.
24. Sternberg K, Gratz M, Koeck K, Mostertz J, Begunk R, Loebler M, Semmling B, Seidlitz A, Hildebrandt P, Homuth G. Magnesium used in bioabsorbable stents controls smooth muscle cell proliferation and stimulates endothelial cells in vitro. J Biomed Mater Res B: Appl Biomater. 2012; 100:41–50. [PubMed: 22114061]
25. Lacolley P, Regnault V, Nicoletti A, Li Z, Michel J-B. The vascular smooth muscle cell in arterial pathology: A cell that can take on multiple roles. Cardiovasc Res. 2012; 95:194–204. [PubMed: 22467316]

26. Cavalcanti-Adam EA, Volberg T, Micoulet A, Kessler H, Geiger B, Spatz JP. Cell spreading and focal adhesion dynamics are regulated by spacing of integrin ligands. Biophys J. 2007; 92:2964–2974. [PubMed: 17277192]
27. Krause A, Cowles EA, Gronowicz G. Integrin-mediated signaling in osteoblasts on titanium implant materials. J Biomed Mater Res. 2000; 52:738–747. [PubMed: 11033557]
28. Roca-Cusachs P, Alcaraz J, Sunyer R, Samitier J, Farré R, Navajas D. Micropatterning of single endothelial cell shape reveals a tight coupling between nuclear volume in G1 and proliferation. Biophys J. 2008; 94:4984–4995. [PubMed: 18326659]
29. Bhadriraju K, Hansen LK. Extracellular matrix- and cytoskeleton-dependent changes in cell shape and stiffness. Exp Cell Res. 2002; 278:92–100. [PubMed: 12126961]
30. Tan JL, Tien J, Pirone DM, Gray DS, Bhadriraju K, Chen CS. Cells lying on a bed of microneedles: An approach to isolate mechanical force. Proc Natl Acad Sci. 2003; 100:1484–1489. [PubMed: 12552122]
31. Wang N, Ostuni E, Whitesides GM, Ingber DE. Micropatterning tractional forces in living cells. Cell Motil Cytoskeleton. 2002; 52:97–106. [PubMed: 12112152]
32. Zreiqat H, Howlett C, Zannettino A, Evans P, Schulze-Tanzil G, Knabe C, Shakibaei M. Mechanisms of magnesium-stimulated adhesion of osteoblastic cells to commonly used orthopaedic implants. J Biomed Mater Res. 2002; 62:175–184. [PubMed: 12209937]
33. Gerthoffer WT. Mechanisms of vascular smooth muscle cell migration. Cir Res. 2007; 100:607–621.
34. Guo H, Lee J-D, Uzui H, Yue H, Wang J, Toyoda K, Geshi T, Ueda T. Effects of folic acid and magnesium on the production of homocysteine-induced extracellular matrix metalloproteinase-2 in cultured rat vascular smooth muscle cells. Cir J. 2006; 70:141–146.
35. Wang G, Ge S, Shen Y, Wang H, Dong Q, Zhang Q, Gao J, Wang Y. Study on the biodegradability and biocompatibility of WE magnesium alloys. Mater Sci Eng C. 2012; 32:2190–2198.
36. Brar HS, Ball JP, Berglund IS, Allen JB, Manuel MV. A study of a biodegradable Mg–3Sc–3Y alloy and the effect of self-passivation on the in vitro degradation. Acta Biomater. 2013; 9:5331–5340. [PubMed: 22902815]
37. Klocke F, Schwade M, Klink A, Veselovac D, Kopp A. Influence of electro discharge machining of biodegradable magnesium on the biocompatibility. Procedia CIRP. 2013; 5:88–93.
38. Li M, Ren L, Li L, He P, Lan G, Zhang Y, Yang K. Cytotoxic effect on osteosarcoma MG-63 cells by degradation of magnesium. J Mater Sci Technol. 2014; 30:888–893.
39. Ren Y, Zhou H, Nabiyouni M, Bhaduri SB. Rapid coating of AZ31 magnesium alloy with calcium deficient hydroxyapatite using microwave energy. Mater Sci Eng C. 2015; 49:364–372.
40. Wei Z, Tian P, Liu X, Zhou B. In vitro degradation, hemolysis, and cytocompatibility of PEO/PLLA composite coating on biodegradable AZ31 alloy. J Biomed Mater Res B: Appl Biomater. 2014; 103:342–354. [PubMed: 24889920]
41. Fletcher DA, Mullins RD. Cell mechanics and the cytoskeleton. Nature. 2010; 463:485–492. [PubMed: 20110992]
42. Vogel SK, Schwille P. Minimal systems to study membrane–cytoskeleton interactions. Curr Opin Biotechnol. 2012; 23:758–765. [PubMed: 22503237]
43. Jones KA, Perkins WJ, Lorenz RR, Prakash Y, Sieck GC, Warner DO. F-actin stabilization increases tension cost during contraction of permeabilized airway smooth muscle in dogs. J Physiol. 1999; 519:527–538. [PubMed: 10457068]
44. Mackman N. Role of tissue factor in hemostasis and thrombosis. Blood Cells Mol Dis. 2006; 36:104–107. [PubMed: 16466951]
45. Spiroski I, Kedev S, Antov S, Trajkov D, Petlichkovski A, Dzhekova-Stojkova S, Kostovska S, Spiroski M. Investigation of SERPINE1 genetic polymorphism in Macedonian patients with occlusive artery disease and deep vein thrombosis. Kardiol Pol. 2009; 67:1088–94. [PubMed: 20017074]
46. Gawaz M, Ott I, Reininger A, Neumann F. Effects of magnesium on platelet aggregation and adhesion. Magnesium modulates surface expression of glycoproteins on platelets in vitro and ex vivo. Thromb Haemost. 1994; 72:912–918. [PubMed: 7740463]

47. Ravn H, Vissinger H, Kristensen S, Husted S. Magnesium inhibits platelet activity–an in vitro study. Thromb Haemost. 1996; 76:88–93. [PubMed: 8819258]

48. Wang J, He Y, Maitz MF, Collins B, Xiong K, Guo L, Yun Y, Wan G, Huang N. A surface-eroding poly (1, 3-trimethylene carbonate) coating for fully biodegradable magnesium-based stent applications: Toward better biofunction, biodegradation and biocompatibility. Acta Biomater. 2013; 9:8678–8689. [PubMed: 23467041]

49. Zhou W, Zheng Y, Leeflang M, Zhou J. Mechanical property, bio-corrosion and in vitro biocompatibility evaluations of Mg–Li–(Al)–(RE) alloys for future cardiovascular stent application. Acta Biomater. 2013; 9:8488–8498. [PubMed: 23385218]

50. Otterbein LE, Soares MP, Yamashita K, Bach FH. Heme oxygenase-1: Unleashing the protective properties of heme. Trends Immunol. 2003; 24:449–455. [PubMed: 12909459]

51. Peyton KJ, Reyna SV, Chapman GB, Ensenat D, Liu X-m, Wang H, Schafer AI, Durante W. Heme oxygenase-1–derived carbon monoxide is an autocrine inhibitor of vascular smooth muscle cell growth. Blood. 2002; 99:4443–4448. [PubMed: 12036874]

52. Galkina E, Ley K. Immune and inflammatory mechanisms of atherosclerosis. Annu Rev Immunol. 2009; 27:165. [PubMed: 19302038]

53. Carter AM. Inflammation, thrombosis and acute coronary syndromes. Diab Vasc Dis Res. 2005; 2:113–121. [PubMed: 16334592]

54. Jung YD, Liu W, Reinmuth N, Ahmad SA, Fan F, Gallick GE, Ellis LM. Vascular endothelial growth factor is upregulated by interleukin-1β in human vascular smooth muscle cells via the p38 mitogen-activated protein kinase pathway. Angiogenesis. 2001; 4:155–162. [PubMed: 11806247]

55. Ulrich CM, Whitton J, Yu J-H, Sibert J, Sparks R, Potter JD, Bigler J. PTGS2 (COX-2)– 765G> C promoter variant reduces risk of colorectal adenoma among nonusers of nonsteroidal anti-inflammatory drugs. Cancer Epidemiol Biomarkers Prev. 2005; 14:616–619. [PubMed: 15767339]

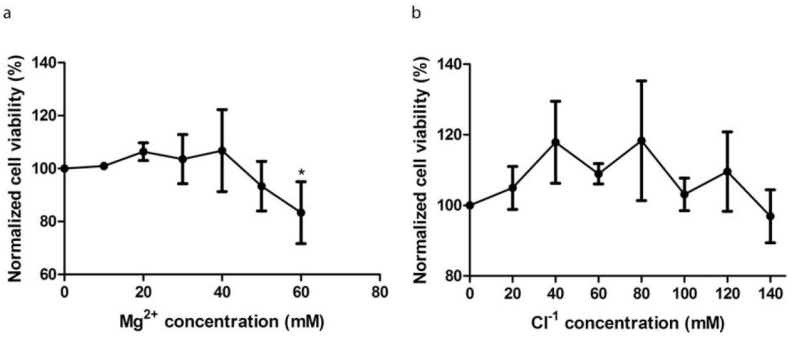

FIGURE 1.

SMC viability analysis. (a) SMC viability was increased by Mg^{2+}, up to 40 m*M* and significantly inhibited at 60 m*M*. (b) Cl^{-1} had no effects on SMC viability. SMCs were seeded and allowed to attach for 24 h, then treated with medium supplementary with different Mg^{2+} concentrations for 24 h. The viability was measured by MTT test. Values were present as mean±SD. *$p<0.05$ with Student's *t* test.

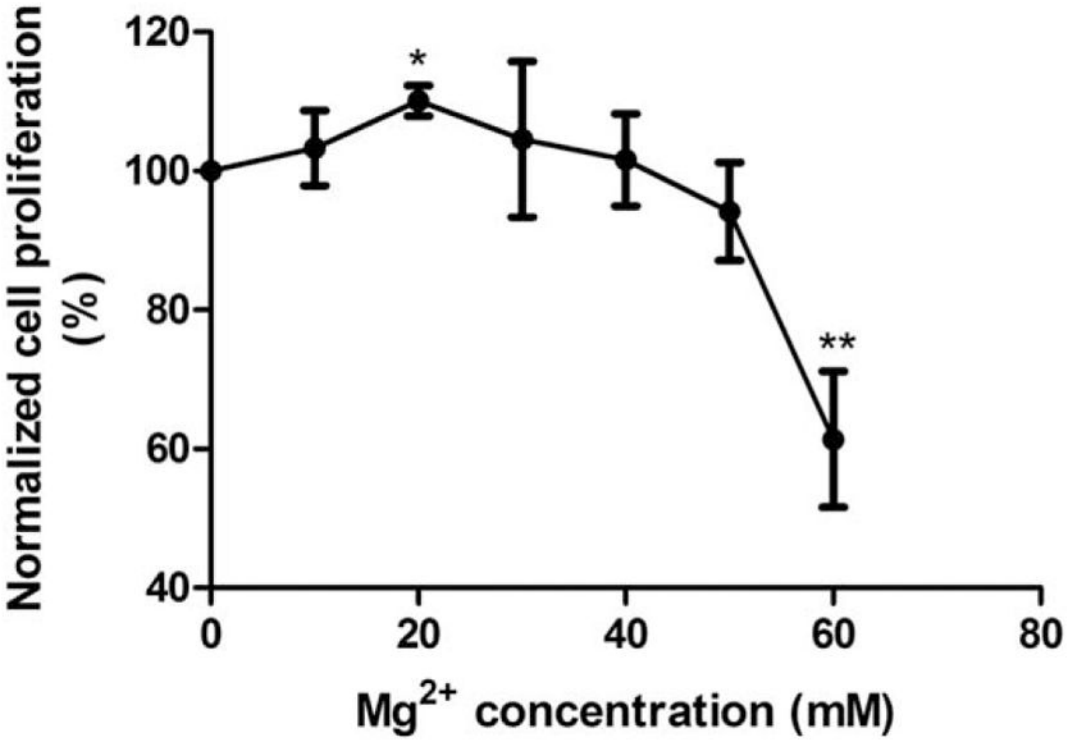

FIGURE 2.

SMC proliferation analysis. Mg^{2+} increased SMC proliferation rate up to 40 m*M*. SMCs were seeded and incubated to allow attachment for 24 h. Then medium was treated with fresh medium supplementary with different Mg^{2+} concentrations for 24 h. The proliferation rate was detected by BrdU assay. All values were present as mean±SD. *p<0.05, **p<0.01, Student's t test.

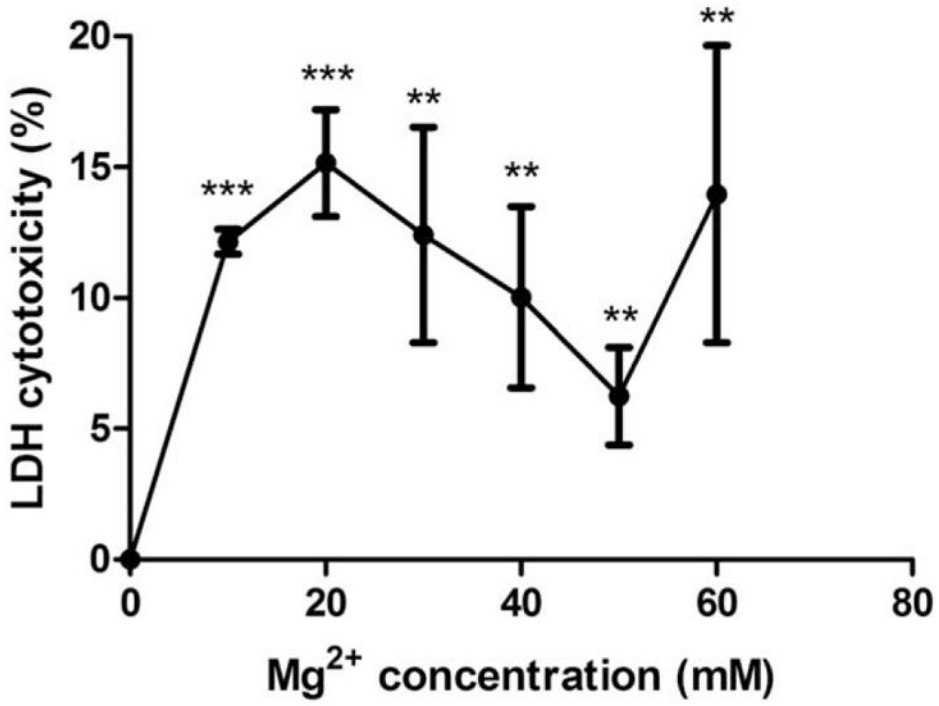

FIGURE 3.

SMC LDH cytotoxicity analysis. Both low and high concentrations Mg^{2+} led to high LDH cytotoxicity. SMCs were seeded and attached for 24 h. Then cells were treated with medium supplementary with different Mg^{2+} concentrations for 24 h. LDH cytotoxicity was measured by a LDH assay kit. All values were present as mean±SD. $^{**}p<0.01$, $^{***}p<0.001$, Student's *t* test.

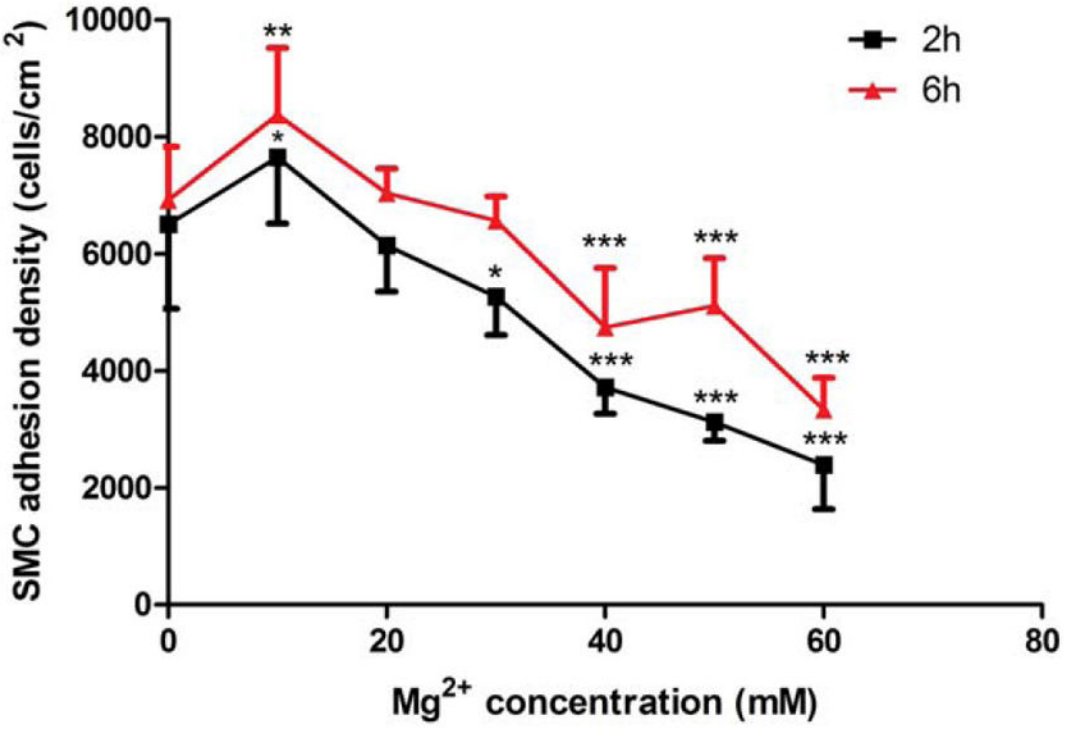

FIGURE 4.

SMC adhesion analysis. 10 m*M* Mg^{2+} increased SMC adhesion at 2 h. At 6 h, 10 m*M* and 20 m*M* Mg^{2+} increased SMC adhesion significantly. SMCs were seeded with medium supplementary with different Mg^{2+} concentrations. At 2 h and 6 h, the medium was removed and washed by DPBS for three times and the adhered cells were counted. At least 10 different fields were counted for each sample. All values were present as mean±SD. **p<0.01, ***p<0.001, Student's t test.

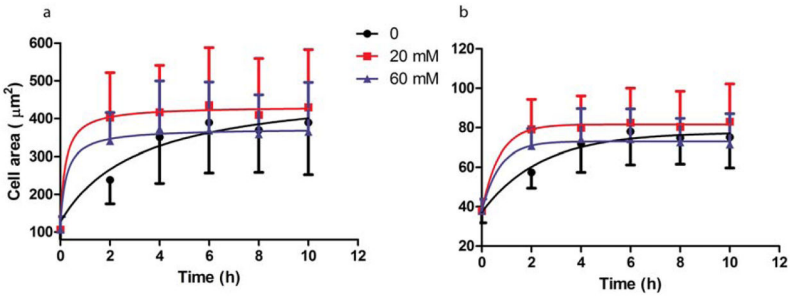

FIGURE 5.

SMC spreading analysis. 20 m*M* Mg^{2+} increased cell area (a) and cell perimeter (b) during the cell spreading process. While 60 m*M* Mg^{2+} increased cell area and perimeter at first, and then were inhibited over time. SMCs were seeded with medium supplementary with different Mg^{2+} concentrations. At different time points, cells were stained with calcein AM. Images were taken and analyzed by Image J.

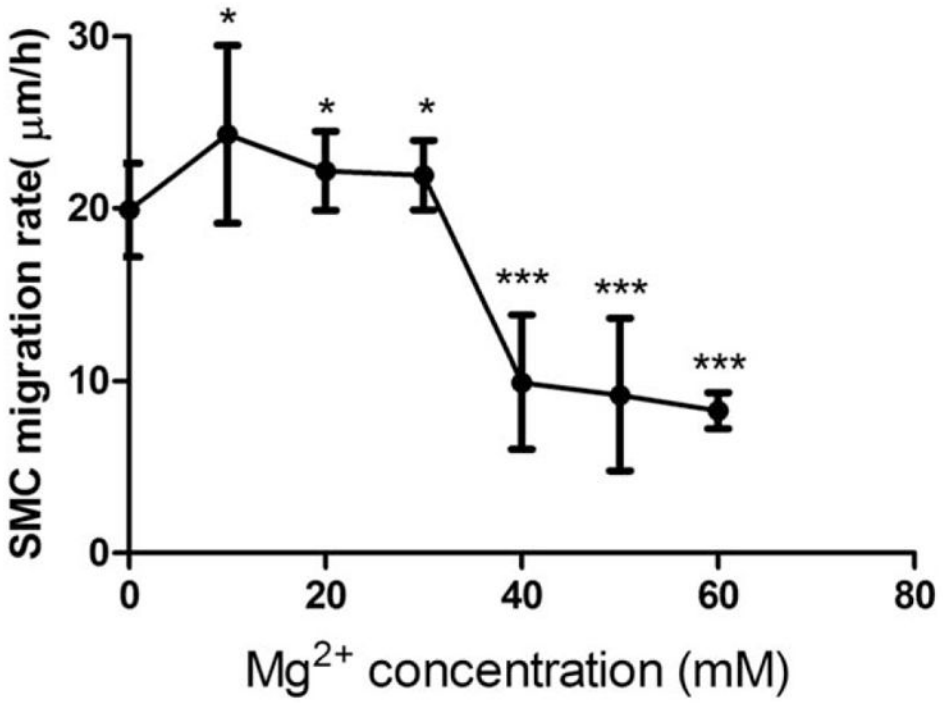

FIGURE 6.

SMC migration analysis. SMC migration rate was significantly enhanced by Mg^{2+}, up to 30 m*M* while inhibited significantly at 40–60 m*M*. SMCs were seeded and a monolayer was formed. Then a P200 pipette tip was used to create a scratch. After washing by DPBS, cells were treated with medium supplementary with different Mg^{2+} concentrations. At time 0 and 6 h, the gaps of the scratch were measured and migration rate was calculated based on the distance SMC migrated. All values were present as mean±SD. *p<0.05, ***p<0.001, Student's t test.

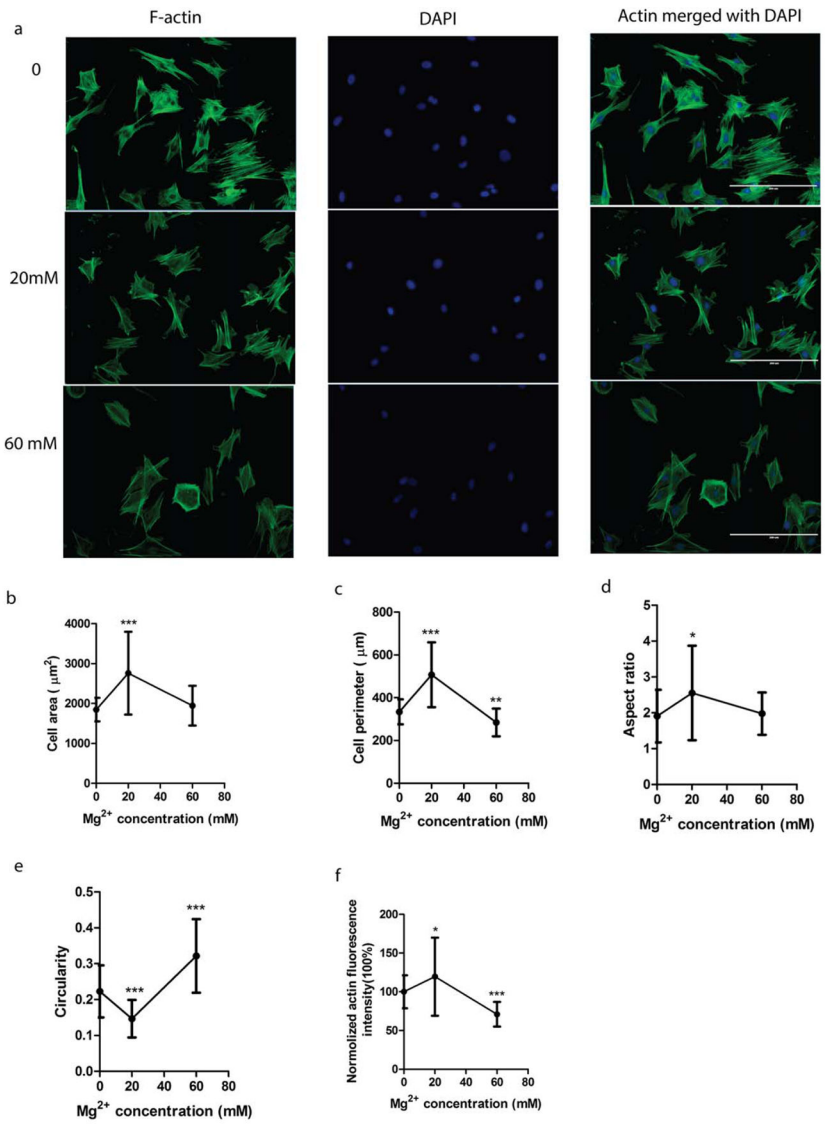

FIGURE 7.

SMC morphology and cytoskeletal analysis. 20 m*M* Mg^{2+} enhanced actin expression and changed the cell morphology into a more elongated shape, while 60 m*M* Mg^{2+} decreased actin expression and changed the cell morphology into a more round shape. (a) The representative figures of actin staining. (b) Cell area was significantly increased by 20 m*M* Mg^{2+}. (c) Cell perimeter was significantly increased by 20 m*M* Mg^{2+} and decreased by 60 m*M* Mg^{2+}. (d) Aspect ratio was significantly increased by 20 m*M* Mg^{2+}. (e) The circularity was decreased by 20 m*M* Mg^{2+} while increased by 60 m*M* Mg^{2+} significantly. (f) The actin expression was enhanced by 20 m*M* Mg^{2+} while inhibited by 60 m*M* Mg^{2+} significantly. *p<0.05, **p<0.01, ***p<0.001, Student's t test. The scale bar was 200 μm.

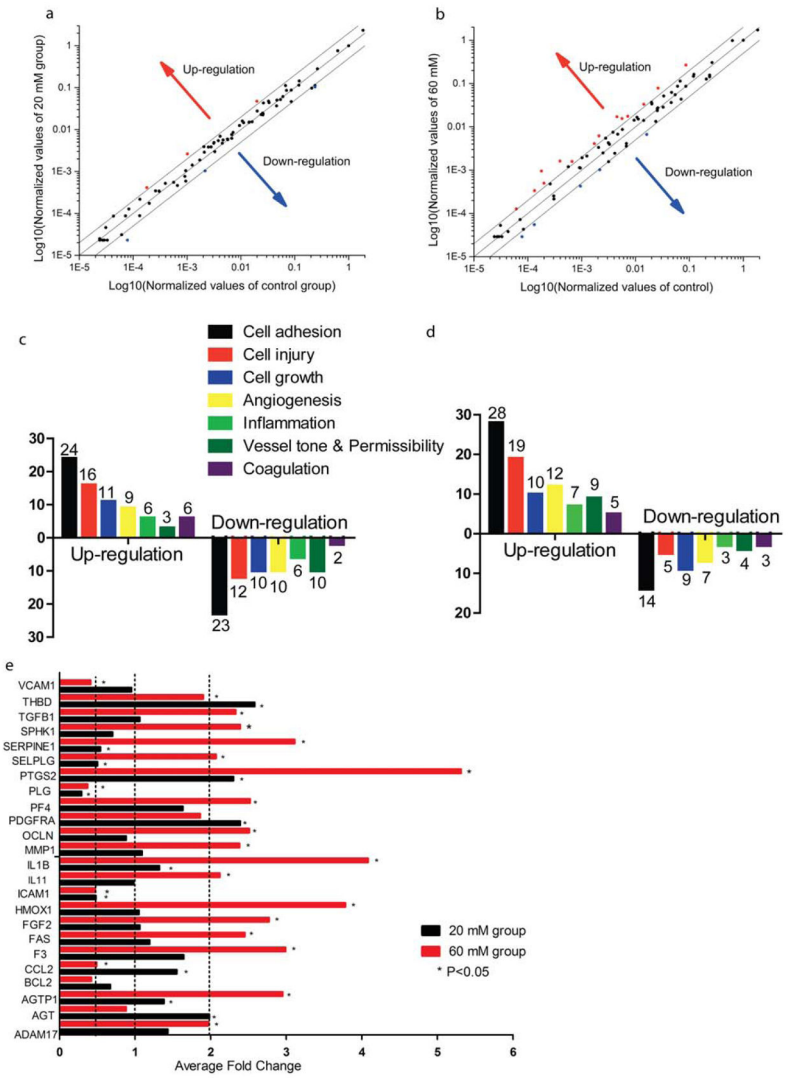

FIGURE 8.

SMC gene expression profile analysis. (a) The scatter plot of gene expression for SMC treated with medium supplementary with 20 m*M* Mg^{2+}. (b) The scatter plot of gene expression for SMC treated with medium supplementary with 60 m*M* Mg^{2+}. (c) The number of genes affected for specific functions when SMCs were treated with medium supplementary with 20 m*M* Mg^{2+}. (d) The number of genes affected for specific functions when SMCs were treated with medium supplementary with 60 m*M* Mg^{2+}. (e) Genes were altered at least twofold when treated with different concentrations of Mg^{2+}. SMCs were seeded and formed a monolayer. Then cells were treated with 20 m*M* or 60 m*M* Mg^{2+} for 24 h. Total RNAs were isolated and cDNAs were synthesized. Then qPCR was used to analyze the gene expression profile. Ct value was <35. **p*<0.05, Student's *t* test.